Synthesis and nanoparticle encapsulation of 3,5-difuranylvinyl-boradiaza-*s*-indacenes for near-infrared fluorescence imaging†

Sehoon Kim,‡ Tymish Y. Ohulchanskyy, Alexander Baev and Paras N. Prasad*

Received 1st August 2008, Accepted 19th February 2009
First published as an Advance Article on the web 31st March 2009
DOI: 10.1039/b813396d

We report molecular design, synthesis, and photophysical study of a series of near-infrared absorbing and fluorescing dyes, 3,5-difuranylvinyl-boradiaza-*s*-indacenes, bearing various 5-membered heteroaromatic heads at the 8-position (FBs). The correlation between the molecular structure and the spectral shift has been studied by quantum chemical calculations at various levels (B3LYP/6-31G*, HF/6-31G* and HF/PM3), which conclude that the planarity determined by the bulkiness of the head unit controls the optical bandgap of FBs, by energetically affecting the lowest unoccupied molecular orbital (LUMO) rather than the highest occupied molecular orbital (HOMO). We also show that incorporation of heavy atoms increased the capability of singlet oxygen generation as a result of enhanced intersystem crossing, which makes FBs potentially useful for near-infrared photodynamic therapy. In vitro near-infrared fluorescence imaging of live tumor cells has been demonstrated through a nanocarrier approach, by encapsulating one of the FB dyes in a stable aqueous formulation of organically modified silica nanoparticles which retains the fluorescence efficiency of the hydrophobic dye in water.

Introduction

Near-infrared (NIR) photonics has great potential as a noninvasive method for biological research, owing to the spectral coincidence with the tissue transparent window (700–1000 nm).[1] Photons in this region are less absorbed and scattered by tissues, which enables deeper light penetration as well as better signal-to-noise ratio by minimal interference from the background autofluorescence. Promising applications include visualization of deep tissues by the near-infrared fluorescence (NIRF) imaging[2] and noninvasive treatment of subcutaneous deep tumors by photodynamic therapy (PDT),[3] both of which are effected by utilizing NIR-active dyes as a fluorescence probe or a singlet oxygen ($^1O_2$)-generating photosensitizer, respectively.

As an effort to develop high-performance fluorescent probes, various classes of difluoroboradiaza-*s*-indacenes (boron dipyrromethene dyes, BODIPYs) have been investigated. BODIPY derivatives are well-known versatile dyes that span the visible spectral region.[4] Due to their advantageous optical properties (high extinction coefficient, high fluorescence quantum yield, and good photostability, etc.), BODIPYs have been utilized for various biophotonic applications such as biological fluorescence probing,[5] ion sensing,[6] and photosensitizing for photodynamic therapy,[7] etc. To extend their application to the NIR range, there have been attempts at wavelength tuning of BODIPYs by structural modification, among which distyryl-substitution at the 3,5-positions has proved to be the most successful way to produce a spectral red shift.[6b,7b,8] Another promising approach is the utilization of pulse NIR lasers for two-photon excitation of BODIPYs.[4]

Recently, we aimed to develop a series of BODIPY derivatives applicable to NIRF imaging. First, in order to achieve efficient spectral red shift, we designed heteroaromatic versions of distyryl-BODIPY, *i.e.*, 3,5-difuranylvinyl-BODIPYs (FBs) with an additional heteroaromatic head unit at the central 8-position (Chart 1). Furan and other 5-membered heteroaromatic rings were chosen for their known beneficial properties, such as good fluorescence capability and lower electron delocalization energy barrier relative to benzene which generally promotes optical bandgap narrowing by lengthening the effective π-conjugation.[9] As another approach toward NIR application, we have also developed a different type of BODIPY with enhanced two-photon absorptivity, which will be reported elsewhere. In this study, we report the synthesis and optical properties of FBs,

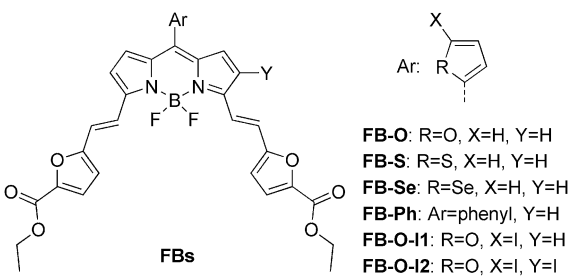

Chart 1 3,5-Difuranylvinyl-boradiaza-*s*-indacenes (FBs)

The Institute for Lasers, Photonics and Biophotonics, Department of Chemistry, State University of New York, Buffalo, New York, 14260-3000, USA

† Electronic supplementary information (ESI) available: The ^{1}H NMR spectra of the prepared compounds. See DOI: 10.1039/b813396d

‡ Present address: Biomedical Research Center, Korea Institute of Science and Technology, 39-1 Hawolgok-dong, Seongbuk-gu, Seoul 136-791, Korea.

together with quantum-chemical calculations for discussions on the correlation between molecular structure and spectral shift. Also presented is the encapsulation of a resulting hydrophobic dye in organically modified silica (ORMOSIL) nanoparticles, to produce cell-permeable delivery formulations. Through this nanocarrier approach, we have demonstrated FB-based NIRF imaging of live tumor cells for potential NIR biophotonic application. In addition, we report efficient singlet oxygen generation under laser excitation, using heavy atom substituted FBs.

Results and discussion

FBs, substituted with phenyl or 5-membered heteroaromatic subunits at the 8-position, were synthesized in moderate-to-high yields by acid-catalyzed condensation and subsequent cyclization with $BF_3 \cdot Et_2O$ between a furanylvinyl-substituted pyrrole (**2**) and aromatic aldehydes (Ar-CHO), following a standard procedure for BODIPY synthesis (Scheme 1).[6–8] Furanyl, thiophenyl, and selenophenyl groups were chosen for the heteroaromatic subunit (Ar in Chart 1), to study the heteroatom effect on the optical properties. FB-O derivatives bearing one and two iodines (FB-O-I1 and FB-O-I2, respectively) were prepared to evaluate the heavy-atom effect[10] which is generally expected to improve the singlet oxygen ($^1O_2$) generation capability for PDT through the enhanced intersystem crossing (ISC) efficiency.[7,11] FB-O-I2 was prepared by iodination of FB-O-I1 in the presence of I_2 and HIO_3. On comparing the coupling constants and splitting patterns in the ^1H NMR spectra of FB-O-I1 and FB-O-I2,[12] as well as from the mass spectrometric results, it has been found that the iodination of FB-O-I1 under the given conditions predominantly gave a product which is mono-iodinated at the 2-position of the central 4-bora-3a,4a-diaza-*s*-indacene ring.

All the obtained FBs exhibit absorption and fluorescence in the deep red and NIR ranges (Fig. 1) with moderate extinction coefficients and fluorescence quantum yields ($\log\varepsilon = 4.79$–4.94, $\Phi_f = 0.05$–0.29). Table 1 summarizes the optical properties of the synthesized FBs in $CHCl_3$, as well as a distyryl derivative (3,5-distyryl-8-phenyl-BODIPY, SB-Ph)[6b] in Et_2O with a solvent polarity similar to $CHCl_3$.[13,14] On comparing the spectral data of FB-Ph and SB-Ph, it is found that the 3,5-difuranylvinyl substitution in place of 3,5-distyryl groups causes a bathochromic shift of ~40 nm, unambiguously attributed to the

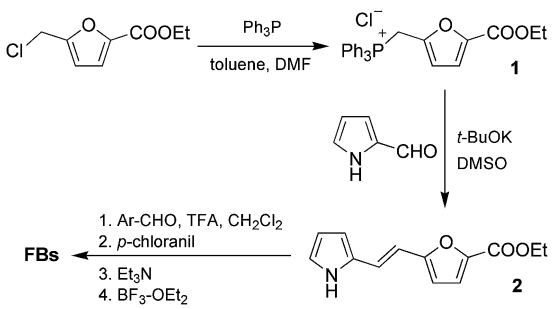

Scheme 1 Synthetic procedures for FB-O, FB-S, FB-Se, FB-Ph, and FB-O-I1, where Ar-CHO is 2-furaldehyde, 2-thiophenecarboxaldehyde, 2-selenophenecarboxaldehyde, benzaldehyde, and 5-iodo-2-furaldehyde, respectively.

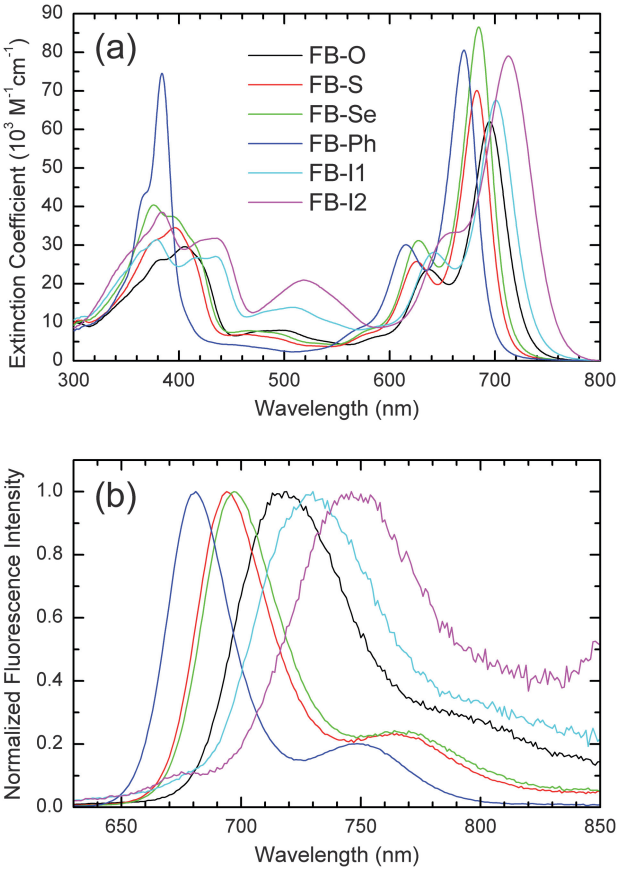

Fig. 1 Absorption (a) and fluorescence (b) spectra of FBs, measured at 5 and 1 μM in $CHCl_3$, respectively ($\lambda_{ex} = 610$ nm).

bandgap narrowing effect of the furan ring due to enhanced π-electron delocalization. Additional substitution of 5-membered heteroaromatic rings (furan, thiophene, and selenophene) in place of the central phenyl head at the 8-position results in a further spectral red shift (>10 nm), where the bathochromic effect is of the order of furan > selenophene ≥ thiophene. As a result, the 5-membered heteroaromatic derivatization produced actually NIR-active BODIPY dyes with fluorescence peaks at around and above 700 nm.

As listed in Table 1, the fluorescence decay rate constants (k_{fl}) are quite similar for all FBs. On the other hand, the nonradiative decay rate constants (k_{nr}) exhibit a correlation with the fluorescence peak wavelength ($\lambda_{max.fl}$), among FB-O, FB-S, and FB-Ph. An increase in k_{nr} (a decrease in Φ_f) is correlated with the red shift of $\lambda_{max.fl}$ (the decrease in fluorescence transition energy), presumably through the energy-gap law,[15] which means that the rate of internal conversion (IC, one of nonradiative decay pathways) increases as the energy gap between two electronic states (S_1 and S_0 in our case) narrows. In the case of FB-Se, a notably high k_{nr} is observed, indicating that the intersystem crossing (ISC) exerts a significant influence on nonradiative decay, due to the presence of a heavy atom (selenium). It is known that the interaction with heavy atoms gives rise to an increase in the spin–orbit interaction which leads to an increase in the rate of spin-forbidden ISC ($S_1 \rightarrow T_n$), and thereby a decrease in the efficiency of the competing radiative transition

Table 1 Photophysical parameters for FBs in $CHCl_3$

	$\lambda_{max.abs}$[a] (nm)	ε_{max}[a] ($M^{-1}cm^{-1}$)	$\lambda_{max.fl}$[b] (nm)	Φ_{fl}[b]	Stokes' shift (cm^{-1})	τ_{fl}[b] (ns)	k_{fl}[c] ($10s^{-1}$)	k_{nr}[c] (10^8s^{-1})
FB-O	695	62 000	718	0.20	461	2.3	0.87	3.48
FB-S	683	70 100	694	0.25	232	2.7	0.93	2.78
FB-Se	685	86 500	697	0.19	251	2.2	0.86	3.68
FB-O-I1	702	67 500	730	0.09	546	1.2	0.75	7.58
FB-O-I2	713	79 100	746	0.05	620	0.6	0.83	15.8
FB-Ph	671	80 500	681	0.29	219	3.5	0.83	2.03
SB-Ph[d]	628	—	641	0.81	323	4.8	1.7	0.4

[a] Measured at 5 μM. [b] Measured at 1 μM. [c] $k_{fl} = \Phi_{fl}/\tau_{fl}$, $k_{nr} = (1 - \Phi_{fl})/\tau_{fl}$. [d] Data for 3,5-distyryl-8-phenyl-BODIPY (SB-Ph) in Et_2O are from ref. 6*b*.

($S_1 \rightarrow S_0$).[10] This heavy-atom effect is seen even more remarkably by the substitution of a heavier atom (iodine). Proportional to the number of iodine (FB-O-I1 and FB-O-I2 in Table 1), iodine incorporation into FB-O leads to significant decreases in Φ_f, along with moderate bathochromic shifts (transition energy decrease), indicating that the rates of ISC and IC increase at the same time by spin–orbit coupling and energy-gap narrowing, respectively, to produce a dramatic increase in k_{nr}.

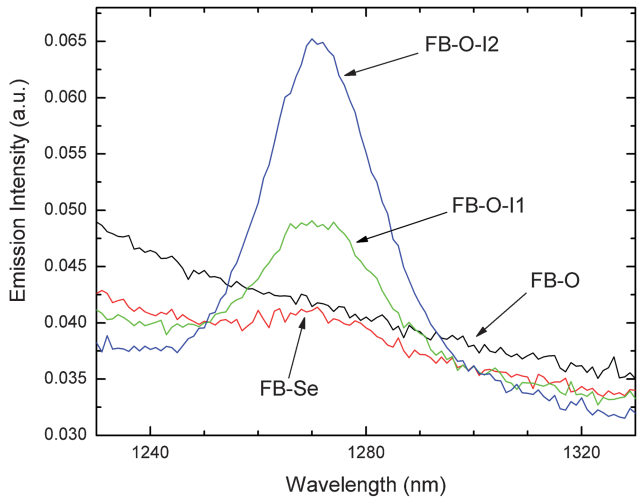

Fig. 2 Phosphorescence spectra of singlet oxygen generated by FBs in $CHCl_3$. The excitation wavelength is 532 nm, at which the absorbances of all samples were matched to ~0.076.

The enhanced ISC efficiency is further evidenced by monitoring the capability of singlet oxygen generation. Singlet oxygen ($^1O_2$) is produced through the reaction between an excited triplet state of a dye and the surrounding molecular oxygen in the triplet ground state ($^3O_2$). Therefore, the efficiency of generation of $^1O_2$ is determined to a great extent by the population of triplet states, *i.e.*, the efficiency of ISC. Highly reactive $^1O_2$ is a key therapeutic species in PDT, killing malignant cells, and the dye capable of producing $^1O_2$-generating triplet states is called a photosensitizer (PS). Fig. 2 shows the phosphorescence spectra of $^1O_2$ at 1270 nm, generated by photoexcited FBs in $CHCl_3$. Notable $^1O_2$ phosphorescence was observed only for the heavy atom-bearing FBs, where the generation efficiency is in the order of FB-O-I2 > FB-O-I1 > FB-Se, as determined by the phosphorescence intensity. This tendency is well correlated with that of k_{nr}, strongly supporting that an increase in k_{nr} by heavy atoms results dominantly from the enhanced ISC rate. The observed capability of singlet oxygen generation suggests a possible application of FBs as NIR-active drugs for PDT.

To gain an insight into quantum-chemical origins determining spectral shifts of FBs, the electronic properties of four model compounds (mFBs in Fig. 3a) were computed by the *ab initio*

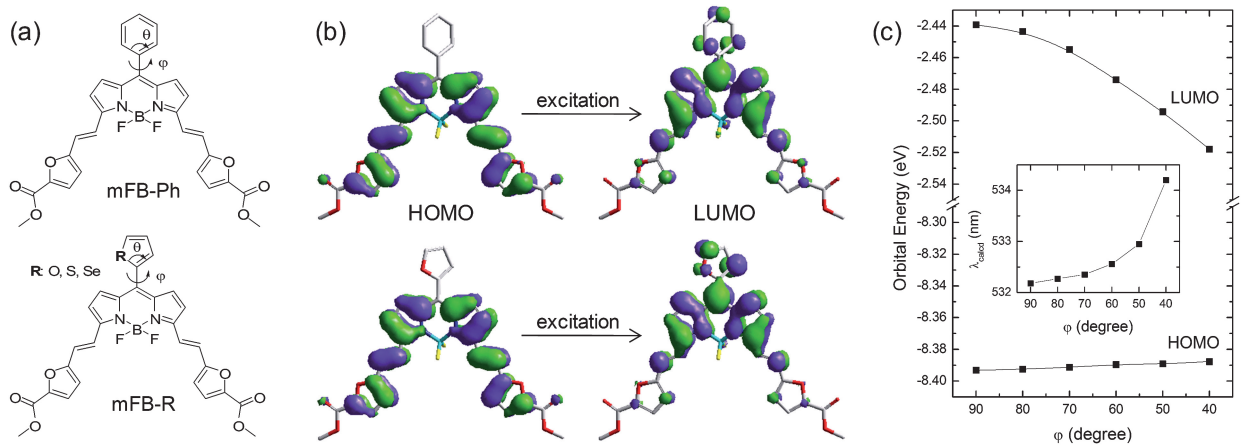

Fig. 3 (a) Model structures (mFBs) used for molecular orbital calculations. (b) HOMO/LUMO diagrams (HF/PM3) for mFB-Ph (top) and mFB-O (bottom). (c) Traces of HOMO–LUMO levels and calculated absorption wavelength (inset) for mFB-Ph, obtained by HF/PM3 as functions of torsion angle (φ in (a)).

Table 2 Calculated geometry parameters, HOMO/LUMO levels (eV), and transition wavelengths, λ_{calcd} (nm)

	B3LYP/6-31G*				HF/6-31G*[b]		HF/PM3[b]	
	θ[a]	φ[a]	HOMO/LUMO	λ_{calcd}	HOMO/LUMO	λ_{calcd}	HOMO/LUMO	λ_{calcd}
mFB-O	108.9°	34.9°	−5.02/−3.04	626	−6.59/−0.47	536	−8.34/−2.70	559
mFB-S	110.1°	47.9°	−5.06/−3.05	618	−6.62/−0.44	531	−8.35/−2.69	554
mFB-Se	110.1°	49.6°	−5.07/−3.07	621	−6.62/−0.45	532	−8.35/−2.74	558
mFB-Ph	118.7°	55.0°	−5.03/−2.97	603	−6.59/−0.31	521	−8.35/−2.57	546

[a] Defined in Fig. 3a. [b] Calculated with B3LYP/6-31G* geometries.

Hartree–Fock self-consistent field method (HF/6-31G*) and the hybrid density functional theory treatment (B3LYP/6-31G*), as well as a semiempirical approach (HF/PM3). The ground-state geometry optimization at the B3LYP/6-31G* level reveals that the structures of common main body (3,5-difuranylvinyl-BODIPY) are planar and almost identical for all mFBs. The aromatic head fragments at the 8-position of BODIPY are twisted out of the main body plane with the torsion angle (φ) depending on the magnitude of steric hindrance between spatially adjacent hydrogen atoms in BODIPY and in head fragments. As listed in Table 2, mFB-Ph shows the largest torsion angle (φ = 55°) among mFBs, since the hexagonal phenyl ring has a larger inner angle (θ = 118.7°) than the heteroaromatic rings, which makes phenyl hydrogens closer to the BODIPY hydrogens at the 1,7-positions, to cause more steric hindrance. In the case of FBs bearing a 5-membered heteroaromatic head unit, the resulting torsion angle (φ) is correlated with the size of the heteroatom, in the order of mFB-O < mFB-S < mFB-Se, indicating that the bigger heteroatom causes an increase of steric hindrance.

As representatively shown by orbital diagrams for mFB-Ph and mFB-O in Fig. 3b, all mFBs have the same patterns of electronic distribution for the highest occupied and the lowest unoccupied molecular orbitals (HOMO and LUMO), which are involved in a main electronic transition (λ_{calcd}) corresponding to the absorption maximum wavelength. In the HOMO, the π-electron distribution is confined within the main body (3,5-difuranylvinyl-BODIPY), whereas in the LUMO it is extended up to the distorted head fragment, suggesting that the energy level of the LUMO might be governed more remarkably by the planarity of the head fragment. The effect of the head planarity on the electronic properties was calculated with mFB-Ph at the HF/PM3 level, by varying its torsion angle (Fig. 3c). With decreasing torsion angle (φ), the HOMO–LUMO gap narrows and the transition wavelength (the inset of Fig. 3c) increases, in a way that the LUMO level is notably stabilized while keeping the HOMO level less affected. This indicates that only the effective π-conjugation of the LUMO is extended by planarization due to the electronic nature of the HOMO and the LUMO, as discussed with Fig. 3b. On comparing mFB-Ph and the other mFBs with a 5-membered heteroaromatic subunit, similar tendencies depending on the head planarity are observed in the calculation results obtained at the levels of B3LYP/6-31G*, HF/6-31G* and HF/PM3 (Table 2). Regardless of the head structure, the HOMO levels are close to each other for all mFBs, suggesting that the head units have a minimal effect on the HOMO due to the absence of electron distribution on them. In contrast, the levels of the LUMO, which has π-electron distribution on the head unit, are notably stabilized with 5-membered heteroaromatic heads over the bulky phenyl unit, due to increased planarity by less bulkiness and other possible electronic effects from the 5-membered ring structure and heteroatoms. As a result, the calculated absorption wavelengths (λ_{calcd}) exhibit the same trends as the experimental ones, which can be correlated with the head planarity in a way that the most planar mFB-O has the longest λ_{calcd}. These calculation results suggest that the derivatization of BODIPY at the 8-position with less bulky π-conjugated segments can be another potential strategy for spectral tuning toward the NIR.

Photostability is another important requirement for dyes to be used for the NIRF imaging applications. In general, NIR fluorescent dyes are labile to photobleaching, since they are mostly composed of photochemically unstable, elongated olefin structures to achieve a narrow optical bandgap.[16] The structures of FBs, however, are rather aromatic and do not carry such long unsaturated hydrocarbon chains, providing an opportunity for better photostability. Among FBs, FB-O seems to be most promising as NIRF imaging probes, with suitable spectral position and quantum yield of fluorescence. Its photostability was examined by comparing with that of a typical NIRF probe,

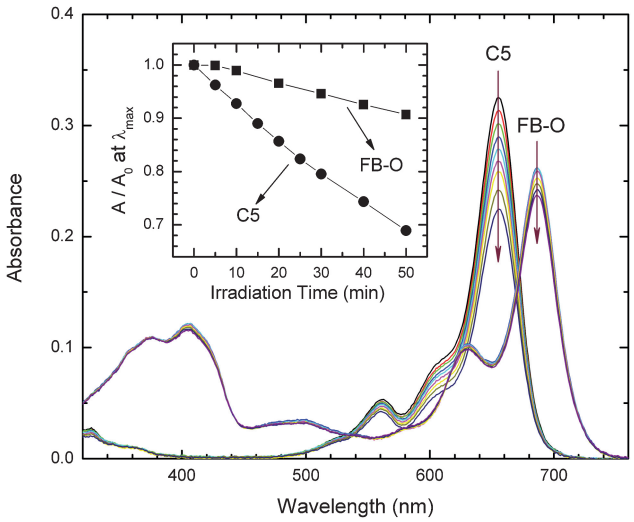

Fig. 4 Comparison of photostability of FB-O and thiadicarbocyanine dye (C5), shown by the change of the absorption spectra in EtOH upon pulse laser illumination (532 nm, 20 Hz, 18 mJ/pulse). The initial absorbance (A_0) at the excitation wavelength was matched to 0.021 for both dye solutions. The inset shows the relative absorbance change (A/A_0) at each λ_{max}, as a function of irradiation time.

thiadicarbocyanine dye (C5).[17] Fig. 4 shows the temporal evolutions of absorption spectra of FB-O and C5 upon repetitive laser illumination. The traces of absorbances at each λ_{max} (the inset of Fig. 4) clearly indicate that FB-O is much more resistant to photobleaching than C5, even with a narrower optical bandgap.

For practical applications of the hydrophobic FBs toward NIRF bioimaging, we attempted encapsulation in a cell-permeable carrier, by utilizing a stable aqueous formulation of organically modified silica (ORMOSIL) nanoparticles.[18,19] Triethoxyvinylsilane (VTES) was used as a silicate precursor, to prepare ORMOSIL nanoparticles encapsulating FB-O (hereafter denoted as OSNP), in the nonpolar core of Tween-80/1-butanol/water micelles. As shown in the transmission electron microscopic (TEM) image of OSNP (Fig. 5a), the obtained nanoparticles are spherical in shape, with a narrow size distribution of 15.2 ± 2.2 nm. Fig. 5b shows the absorption and fluorescence spectra of an aqueous suspension of OSNP. The band shapes and the peak positions ($\lambda_{max.abs}$ = 695 nm and $\lambda_{max.fl}$ = 719 nm) are almost identical to those of the $CHCl_3$ solution, with no sign for any self-aggregation of FB-O. Note that in water, hydrophobic FBs are not soluble and form aggregates with changed absorption and quenched fluorescence, as observed for common organic dyes.[20] Consequently, the efficient NIR fluorescence from an aqueous suspension of OSNP indicates that the FB-O molecules have successfully been embedded in the hydrophobic part of the ORMOSIL matrix, in the molecularly dispersed form.

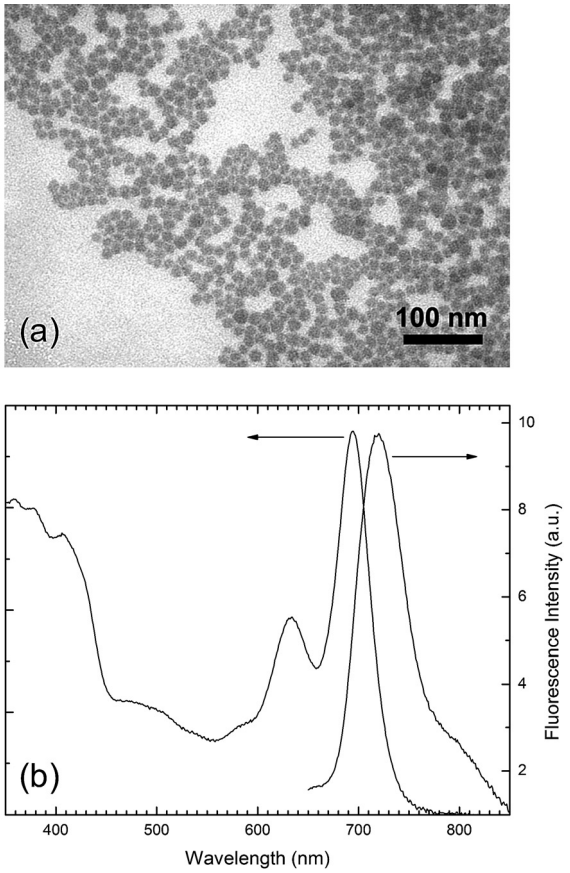

Fig. 5 TEM image (a) and absorption/fluorescence spectra (b) of ORMOSIL nanoparticles encapsulating FB-O (OSNP).

The potential of FB-O as a NIR fluorescent probe was evaluated in vitro by fluorescence imaging of live tumor cells, in the nanoassembled form of OSNP. Fig. 6 shows the microscopic images of Cos-1 cells treated with an aqueous formulation of OSNP, where for the confocal fluorescence image only the NIR signal above 750 nm was taken using a longpass 750LP filter. An intense NIR fluorescence signal is observed from the cells (Fig. 6b), indicating an active uptake of OSNP by tumor cells. As shown in the merged transmission and fluorescence images (Fig. 6c), the intracellular uptake pattern of OSNP is quite similar to those of other ORMOSIL nanoparticles,[18,19] with significant accumulation in the cytoplasm. This in vitro demonstration of NIRF imaging suggests the potential utility of 3,5-difuranylvinyl-BODIPYs for NIR biophotonics.

Conclusion

Novel NIR-absorbing and fluorescing boradiaza-*s*-indacene (BODIPY) dyes, with and without heavy atoms, have been designed, synthesized, and photophysically investigated. Spectral red shift of the BODIPY chromophore has successfully been achieved up to the NIR region at around and above 700 nm, through the heteroaromatic derivatization by incorporating difuranylvinyl groups at the 3,5-positions as well as another 5-membered heteroaromatic head at the 8-position. It has been concluded from quantum chemical calculations that the planarity determined by the bulkiness of the head unit plays an important role in achieving further spectral red shift of FBs. A cell-permeable NIRF imaging nanoprobe has successfully been prepared, by encapsulating one FB dye in ORMOSIL

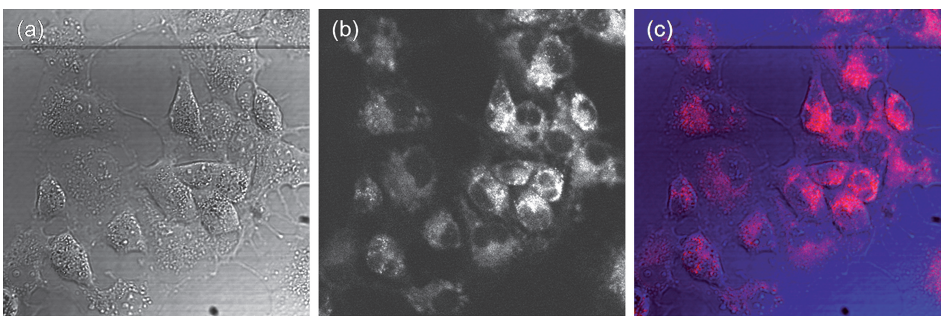

Fig. 6 Transmission (a), fluorescence (b) and merged (c) images of Cos-1 cells stained with OSNP. In the merged image, transmission and fluorescence signals are shown in blue and red, respectively.

nanoparticles while retaining its fluorescence efficiency. It has been demonstrated by heavy atom-effected singlet oxygen generation and in vitro cellular NIRF imaging that our hetero-aromatized BODIPY dyes hold considerable potential for NIR biophotonic applications.

Experimental

Chemical structures were identified by ^{1}H NMR (Varian INOVA-400, 400 MHz) and electrospray ionization (ESI) mass spectra (Themo Finnigan LCQ Advantage mass spectrometer). Cosurfactant 1-butanol and NH_4OH (28.0∼30.0%) are products of J. T. Baker. All other chemicals used were purchased from Aldrich. UV-vis absorption and fluorescence spectra were recorded using a Shimadzu UV-3600 spectrophotometer and a Jobin-Yvon Fluorog FL-311 spectrofluorometer, respectively. Relative fluorescence quantum yields (Φ_f) were estimated using 3,3′-diethylthiadicarbocyanine iodide (C5) in ethanol ($\Phi_f = 0.35$) as a reference.[17] Fluorescence decays were obtained by using an EasyLife fluorescence lifetime system (Photon Technology International, Birmingham, NJ). Singlet oxygen luminescence spectra peaking at 1270 nm were recorded by using a SPEX 270M spectrometer (Jobin Yvon) equipped with an InGaAs photodetector (Electro-Optical Systems Inc.), under the excitation at 532 nm from the diode-pumped solid-state laser (Millenia, Spectra-Physics).

2-Selenophenecarboxaldehyde

To a solution of selenophene (3 g, 22.9 mmol) in DMF (14 mL), phosphorus oxychloride (5.6 mL, 60 mmol) was added and heated for 2 hrs at 85 °C. After cooling, the resulting mixture was poured onto excess ice-cold water, neutralized with sodium acetate and heated to boil. The cooled mixture was extracted with ethyl acetate. The organic extracts were washed with brine and dried over $MgSO_4$. The crude product obtained after solvent evaporation was purified by column chromatography on silica gel (ethyl acetate/*n*-hexane = 1/3). Yield 2 g (55%). ^{1}H NMR ($CDCl_3$): δ 9.82 (s, 1H), 8.50 (d, 1H, J = 5.2 Hz), 8.03 (d, 1H, J = 4.0 Hz), 7.48 (m, 1H).

2-(2-{5-[Ethoxycarbonyl]-furan-2-yl}vinyl)-1*H*-pyrrole (2)

A mixture of ethyl 5-(chloromethyl)-2-furancarboxylate (4 g, 21.2 mmol) and triphenylphosphine (8.34 g, 31.8 mmol) in toluene (30 mL) was refluxed for 5 hrs in the presence of 0.3 mL of DMF. After cooling, the precipitate was filtered off and washed with diethyl ether, to give 7.5 g of pure ({5-[ethoxycarbonyl]furan-2-yl}methyl)triphenylphosphonium chloride (**1**, 78%). To a solution of potassium *t*-butoxide (1.1 g, 9.8 mmol) in DMSO (8 mL) was added the triphenylphosphonium salt **1** (4 g, 8.9 mmol) at room temperature. The mixture was stirred for 20 min or until complete dissolution of the salt. Then, pyrrole-2-carboxaldehyde (0.93 g, 9.8 mmol) dissolved in DMSO (8 mL) was added dropwise to the ylide solution. After overnight stirring at room temperature, the mixture was poured into water and extracted with ethyl acetate. The organic extracts were washed with brine, and dried over $MgSO_4$. The crude product obtained after solvent evaporation was purified by column chromatography on silica gel (ethyl acetate/*n*-hexane = 1/4), and then recrystallized from *n*-hexane, to give a trans isomer of compound **2**. Yield 0.8 g (39%). ^{1}H NMR ($CDCl_3$): δ 7.16 (d, 1H, J = 3.6 Hz), 7.13 (d, 1H, J = 16.4 Hz), 6.86 (m, 1H), 6.48 (d, 1H, J = 16.4 Hz), 6.44 (m, 1H), 6.33 (d, 1H, J = 3.6 Hz), 6.27 (m, 1H), 4.37 (q, 2H, J = 7.2 Hz), 1.39 (t, 3H, J = 7.2 Hz).

General procedure for difluoroboradiaza-*s*-indacene (BODIPY) formation

Compound **2** (0.2 g, 0.86 mmol) and aromatic aldehyde (Ar-CHO, 0.43 mmol) in CH_2Cl_2 (15 mL) were stirred in the presence of 1 drop of trifluoroacetic acid (TFA) at room temperature for 5 hrs. *p*-Chloranil (tetrachloro-1,4-benzoquinone, 0.212 g, 0.86 mmol) in CH_2Cl_2 (10 mL) was added, and the mixture was stirred for 20 min. Then, triethylamine (1 mL) and $BF_3{\cdot}OEt_2$ (1 mL) were added slowly in sequence. After stirring for another 5 hrs, the diluted mixture with excess CH_2Cl_2 was washed with water, and dried over $MgSO_4$. The crude product obtained after solvent evaporation was purified by column chromatography on a silica gel (ethyl acetate/CH_2Cl_2 = 1/6), and then reprecipitated from CH_2Cl_2 into *n*-hexane, to give pure FBs.

3,5-Bis(2-{5-[ethoxycarbonyl]-furan-2-yl}vinyl)-8-(furan-2-yl)-BODIPY (FB-O)

0.15 g isolated. Yield 59%. ^{1}H NMR ($CDCl_3$): δ 7.77 (m, 1H), 7.74 (d, 2H, J = 16.4 Hz), 7.36 (d, 2H, J = 4.0 Hz), 7.25 (d, 2H, J = 3.6 Hz), 7.20 (d, 2H, J = 16.4 Hz), 7.01 (m, 1H), 6.94 (d, 2H, J = 4.0 Hz), 6.85 (d, 2H, J = 3.6 Hz), 6.68 (m, 1H), 4.41 (q, 4H, J = 7.2 Hz), 1.42 (t, 6H, J = 7.2 Hz). MS (EI): calcd for $C_{31}H_{25}BF_2N_2O_7$, m/z = 586.17; found, m/z = 586.4. Anal. calcd for $C_{31}H_{25}BF_2N_2O_7$: C, 63.50; H, 4.30; N, 4.78. Found: C, 63.7; H, 4.3; N, 4.7%.

3,5-Bis(2-{5-[ethoxycarbonyl]-furan-2-yl}vinyl)-8-(thiophen-2-yl)-BODIPY (FB-S)

0.187 g isolated. Yield 72%. ^{1}H NMR ($CDCl_3$): δ 7.72 (d, 2H, J = 16.4 Hz), 7.62 (d, 1H, J = 4.8 Hz), 7.43 (d, 1H, J = 3.2 Hz), 7.24–7.22 (m, 3H), 7.19 (d, 2H, J = 16.4 Hz), 7.15 (d, 2H, J = 4.4 Hz), 6.91 (d, 2H, J = 4.4 Hz), 6.84 (d, 2H, J = 3.6 Hz), 4.41 (q, 4H, J = 7.2 Hz), 1.42 (t, 6H, J = 7.2 Hz). MS (EI): calcd for $C_{31}H_{25}BF_2N_2O_6S$, m/z = 602.15; found, m/z = 602.1. Anal. calcd for $C_{31}H_{25}BF_2N_2O_6S$: C, 61.81; H, 4.18; N, 4.65. Found: C, 61.5; H, 4.1; N, 4.7%.

3,5-Bis(2-{5-[ethoxycarbonyl]-furan-2-yl}vinyl)-8-(selenophen-2-yl)-BODIPY (FB-Se)

0.189 g isolated. Yield 67%. ^{1}H NMR ($CDCl_3$): δ 8.33 (d, 1H, J = 5.6 Hz), 7.72 (d, 2H, J = 16.8 Hz), 7.59 (d, 1H, J = 3.2 Hz), 7.46 (m, 1H), 7.23 (d, 2H, J = 3.6 Hz), 7.19 (d, 2H, J = 16.8 Hz), 7.16 (d, 2H, J = 4.4 Hz), 6.90 (d, 2H, J = 4.4 Hz), 6.84 (d, 2H, J = 3.6 Hz), 4.41 (q, 4H, J = 7.2 Hz), 1.42 (t, 6H, J = 7.2 Hz). MS (EI): calcd for $C_{31}H_{25}BF_2N_2O_6Se$, m/z = 650.09; found, m/z = 650.1. Anal. calcd for $C_{31}H_{25}BF_2N_2O_6Se$: C, 57.34; H, 3.88; N, 4.31. Found: C, 57.1; H, 3.8; N, 4.4%.

3,5-Bis(2-{5-[ethoxycarbonyl]-furan-2-yl}vinyl)-8-phenyl-BODOPY (FB-Ph)

0.067 g isolated. Yield 26%. ^{1}H NMR ($CDCl_3$): δ 7.73 (d, 2H, J = 16.8 Hz), 7.54-7.49 (m, 5H), 7.24 (d, 2H, J = 3.6 Hz), 7.19 (d, 2H, J = 16.8 Hz), 6.88 (d, 2H, J = 4.4 Hz), 6.84 (d, 2H, J = 3.6 Hz), 6.82 (d, 2H, J = 4.4 Hz), 4.41 (q, 4H, J = 7.2 Hz), 1.42 (t, 6H, J = 7.2 Hz). MS (EI): calcd for $C_{33}H_{27}BF_2N_2O_6$, m/z = 596.19; found, m/z = 596.4. Anal. calcd for $C_{33}H_{27}BF_2N_2O_6$: C, 66.46; H, 4.56; N, 4.70. Found: C, 66.3; H, 4.5; N, 4.7%.

3,5-Bis(2-{5-[ethoxycarbonyl]-furan-2-yl}vinyl)-8-(5-iodofuran-2-yl)-BODIPY (FB-O-I1)

0.146 g isolated. Yield 47%. ^{1}H NMR ($CDCl_3$): 7.72 (d, 2H, J = 16.4 Hz), 7.30 (d, 2H, J = 4.4 Hz), 7.23 (d, 2H, J = 3.6 Hz), 7.19 (d, 2H, J = 16.4 Hz), 6.94 (d, 2H, J = 4.4 Hz), 6.87 (d, 1H, J = 3.6 Hz), 6.84 (d, 2H, J = 3.6 Hz), 6.81 (d, 1H, J = 3.6 Hz), 4.41 (q, 4H, J = 7.2 Hz), 1.42 (t, 6H, J = 7.2 Hz). MS (EI): calcd for $C_{31}H_{24}BF_2IN_2O_7$, m/z = 712.07; found, m/z = 712.1. Anal. calcd for $C_{31}H_{24}BF_2IN_2O_7$: C, 52.28; H, 3.40; N, 3.93. Found: C, 52.0; H, 3.3; N, 4.0%.

2-Iodo-3,5-bis(2-{5-[ethoxycarbonyl]-furan-2-yl}vinyl)-8-(5-iodofuran-2-yl)-BODIPY (FB-O-I2)

To a mixture of FB-I1 (0.1 g, 0.14 mmol) and iodine (0.178 g, 0.7 mmol) dissolved in DMF (4 mL) was added iodic acid (0.1 g, 0.57 mmol) solution in water (0.3 mL) with stirring over 5 min. After overnight stirring at room temperature, the diluted mixture with excess CH_2Cl_2 was washed with saturated sodium thiosulfate solution and brine to remove excess iodine and DMF, and then dried over $MgSO_4$. The crude product obtained after solvent evaporation was recrystallized from ethyl acetate, to give FB-I2. Yield 0.03 g (51%). ^{1}H NMR ($CDCl_3$): 7.93 (d, 1H, J = 17.2 Hz), 7.69 (d, 1H, J = 18.0 Hz), 7.65 (d, 1H, J = 17.2 Hz), 7.44 (s, 1H), 7.37 (d, 1H, J = 4.4 Hz), 7.23 (d, 2H, J = 3.6 Hz), 7.21 (d, 1H, J = 18.0 Hz), 6.98 (d, 1H, J = 4.4 Hz), 6.90 (d, 1H, J = 3.6 Hz), 6.86 (d, 1H, J = 3.6 Hz), 6.83 (d, 2H, J = 3.6 Hz), 4.41 (q, 4H, J = 7.2 Hz), 1.42 (t, 6H, J = 7.2 Hz). MS (EI): calcd for $C_{31}H_{23}BF_2I_2N_2O_7$, m/z = 837.97; found, m/z = 838.0. Anal. calcd for $C_{31}H_{23}BF_2I_2N_2O_7$: C, 44.42; H, 2.77; N, 3.34. Found: C, 44.1; H, 2.7; N, 3.4%.

Calculation details

The ground-state geometries of the model structures were optimized by means of the Gaussian electronic structure program,[21] making use of the density functional theory (DFT) method with a hybrid functional B3LYP and a split-valence basis set 6-31G*. The calculations of electronic properties at various levels were carried out with the B3LYP/6-31G*-optimized geometries, using the DALTON program[22] (B3LYP/6-31G* and HF/6-31G*) and the HyperChem 7.5 program (HF/PM3). The linear response theory applied to either single-determinant self-consistent field reference state (HF) or Kohn–Sham reference state (DFT) was applied to calculate absorption wavelengths. For the head planarity-dependent electronic properties of mFB-Ph (Fig. 3c), the configuration interaction calculations were performed with 129 configurations (HF/PM3), by changing the torsion angle (φ) of the B3LYP/6-31G*-optimized geometry.

Encapsulation of FB-O in ORMOSIL nanoparticles

The aqueous micelle was prepared by dissolving 0.2 g of Tween-80 and 0.3 mL of 1-butanol in 10 mL of deionized water by vigorous magnetic stirring. Then, 60 μL of FB-O solution in DMSO (5 mM) and 200 μL of neat VTES were added to the micellar solution under magnetic stirring, and the resulting mixture was sonicated for about 5 min, or until they became homogeneous. After that, 40 μL of NH_4OH was added and the mixture was magnetically stirred for about 20 hrs at room temperature, to ensure completion of sol-gel condensation. The residual DMSO, catalyst and surfactants were removed by dialyzing the nanoparticle dispersion against deionized water in a 12–14 kDa cutoff cellulose membrane (Spectrum Laboratories, Inc.) for 48 h. To further remove the residual Tween-80, the dialyzed dispersions were spin-filtered in a microfuge membrane filter (NANOSEP 100K OMEGA, Pall Corporation) by centrifuging at 11 000 rpm for 40 min. Nanoparticles collected on the membrane were redispersed in water of the same volume as the amount before spin filtration.

In-vitro studies with tumor cells: nanoparticle uptake and NIRF imaging

For studying nanoparticles uptake and imaging, Cos-1 cells were used, maintained in DMEM medium with 10% fetal bovine serum (FBS) and appropriate antibiotic. The cells at a confluency of 70–75% were treated overnight with the nanoparticles. Next day, the treated cells were washed thoroughly with PBS and then directly imaged using a confocal laser scanning microscope (MRC-1024, Bio-Rad, Richmond, CA). A water immersion objective lens (Nikon, Fluor-60X, NA = 1.0) was used for cell imaging. A Ti:sapphire laser (Tsunami from Spectra-Physics) pumped by a diode-pumped solid state laser (Millenia, Spectra-Physics) was used as a source of excitation. The Ti:sapphire output, tuned to 725 nm, was coupled into a single mode fiber for delivery into the confocal scan head. Long-pass filters, 585 LP (585 nm) and 750 LP (750 nm), were used as emission filters for NIR fluorescence imaging.

Acknowledgements

This work was supported by grant from the National Institute of Health (R01CA119358) and the John R. Oishei Foundation.

References

1 P. N. Prasad, *Introduction to Biophotonics*; John Wiley & Sons: Hoboken, New Jersey, 2003.
2 R. Weissleder and V. Ntziachristos, *Nat. Med.*, 2003, **9**, 123.
3 (*a*) B. W. Henderson; T. J. Dougherty, *Photodynamic Therapy: Basic Principles and Clinical Applications*; Marcel Dekker: New York, 1992. 507; (*b*) T. J. Dougherty, C. J. Gomer, B. W. Henderson, G. Jori, D. Kessel, M. Korbelik, J. Moan and Q. Peng, *J. Natl. Cancer Inst.*, 1998, **90**, 889; (*c*) D. E. J. G. J. Dolmans, D. Fukumura and R. K. Jain, *Nature Reviews Cancer*, 2003, **3**, 380.
4 R. P. Haugland, *Handbook of Fluorescent Probes and Research Products*, 9th edn.; Molecular Probes Inc.: Eugene, 2002.
5 (*a*) D. Dahim, N. K. Mizuno, X.-M. Li, W. E. Momsen, M. M. Momsen and H. L. Brockman, *Biophys. J.*, 2002, **83**, 1511;

(*22*) M. Yee, S. C. Fas, M. M. Stohlmeyer, T. J. Wandless and K. A. Cimprich, *J. Biol. Chem.*, 2005, **280**, 29053.

6 (*a*) K. Rurack, M. Kollmannsberger, U. Resch-Genger and J. Daub, *J. Am. Chem. Soc.*, 2000, **122**, 968; (*b*) K. Rurack, M. Kollmannsberger and J. Daub, *New J. Chem.*, 2001, **25**, 289; (*c*) A. Coskun and E. U. Akkaya, *Tetrahedron Lett.*, 2004, **45**, 4947; (*d*) A. Coskun and E. U. Akkaya, *J. Am. Chem. Soc.*, 2005, **127**, 10464; (*e*) M. Baruah, W. Qin, C. Flors, J. Hofkens, R. A. L. Vallée, D. Beljonne, M. Van der Auweraer, W. M. De Borggraeve and N. Boens, *J. Phys. Chem. A*, 2006, **110**, 5998; (*f*) X. Qi, E. J. Jun, L. Xu, S.-J. Kim, J. S. J. Hong, Y. J. Yoon and J. Yoon, *J. Org. Chem.*, 2006, **71**, 2881.

7 (*a*) T. Yogo, Y. Urano, Y. Ishitsuka, F. Maniwa and T. Nagano, *J. Am. Chem. Soc.*, 2005, **127**, 12162; (*b*) S. Atilgan, Z. Ekmekci, A. L. Dogan, D. Guc and E. U. Akkaya, *Chem. Commun.*, 2006, 4398.

8 (*a*) Z. Dost, S. Atilgan and E. U. Akkaya, *Tetrahedron*, 2006, **62**, 8484; (*b*) T. Rohand, W. Qin, N. Boens and W. Dehaen, *Eur. J. Org. Chem.*, 2006, 4658.

9 P. R. Varanasi, A. K.-Y. Jen, J. Chandrasekhar, I. N. N. Namboothiri and A. Rathna, *J. Am. Chem. Soc.*, 1996, **118**, 12443.

10 N. J. Turro, *Modern Molecular Photochemistry*; Benjamin: Menlo Park, 1978.

11 (*a*) A. Gorman, J. Killoran, C. O'Shea, T. Kenna, W. M. Gallagher and D. F. O'Shea, *J. Am. Chem. Soc.*, 2004, **126**, 10619; (*b*) T. Y. Ohulchanskyy, D. J. Donnelly, M. R. Detty and P. N. Prasad, *J. Phys. Chem. B*, 2004, **108**, 8668.

12 The ^{1}H NMR spectrum of FB-O-I1 shows that the aromatic resonances are split into doublets with different coupling constants (*J*): 3.6 Hz for iodo- and ethylcarboxy-furan rings (four peaks, six protons) and 4.4 Hz for the central 4-bora-3a,4a-diaza-*s*-indacene (BODIPY) ring (two peaks, four protons). In the ^{1}H NMR spectrum of FB-O-I2, the number, coupling constants, and splitting patterns of furan proton peaks werekept the same, while the peak pattern of BODIPY protons was changed into two doublets for two protons ($J = 4.4$ Hz) and a singlet for one proton. This comparison indicates that one proton of the BODIPY ring was replaced by iodination at the 2-position, similar to the reported synthesis in ref. 7*a*,*b*.

13 (*a*) N. Mataga, Y. Kaifu and M. Koizumi, *Bull. Chem. Soc. Jpn.*, 1956, **29**, 465; (*b*) E. Lippert, *Z. Naturforsch., A: Phys. Sci.*, 1955, 541.

14 Solvent polarity parameters (Δf) of $CHCl^3$ for FB-Ph and diethylether for SB-Ph are 0.253 and 0.256, respectively. Δf is defined in ref. 13 as $[(\varepsilon - 1)/(2\varepsilon + 1) - 0.5(n^2 - 1)/(2n^2 + 1)]$, where ε and n denote the static dielectric constant and the refractive index, respectively.

15 (*a*) H. Fidder, M. Rini and E. T. J. Nibbering, *J. Am. Chem. Soc.*, 2004, **126**, 3789; (*b*) S. Nagaoka, A. Nakamura and U. Nagashima, *J. Photochem. Photobiol. A*, 2002, **154**, 23.

16 *Handbook of Confocal Microscopy*, 2nd ed.; Pawley, J. B., Ed.; Plenum Press: New York, 1995.

17 D. N. Dempster, T. Morrow, R. Rankin and G. F. Thompson, *J. Chem. Soc., Faraday Trans. 2*, 1972, **68**, 1479.

18 (*a*) I. Roy, T. Y. Ohulchanskyy, H. E. Pudavar, J. E. Bergey, A. R. Oseroff, J. Morgan, T. J. Dougherty and P. N. Prasad, *J. Am. Chem. Soc.*, 2003, **125**, 7860; (*b*) I. Roy, T. Y. Ohulchanskyy, D. J. Bharali, H. E. Pudavar, R. A. Mistretta, N. Kaur and P. N. Prasad, *Proc. Natl. Acad. Sci. USA*, 2005, **102**, 279; (*c*) T. Y. Ohulchanskyy, I. Roy, L. N. Goswami, Y. Chen, E. J. Bergey, R. K. Pandey, A. R. Oseroff and P. N. Prasad, *Nano Lett.*, 2007, **7**, 2835.

19 (*a*) S. Kim, T. Y. Ohulchanskyy, H. E. Pudavar, R. K. Pandey and P. N. Prasad, *J. Am. Chem. Soc.*, 2007, **129**, 2669; (*b*) S. Kim, H. E. Pudavar, A. Bonoiu and P. N. Prasad, *Adv. Mater.*, 2007, **19**, 3791; (*c*) S. Kim, H. Huang, H. E. Pudavar, Y. Cui and P. N. Prasad, *Chem. Mater.*, 2007, **19**, 5650.

20 J. B. BirksIn *Photophysics of Aromatic Molecules*; Wiley: London, 1970.

21 M. J. Frisch; G. W. Trucks; H. B. Schlegel; G. E. Scuseria; M. A. Robb; J. R. Cheeseman; V. G. Zakrzewski; J. A. Montgomery, Jr.; R. E. Stratmann; J. C. Burant; S. Dapprich; J. M. Millam; A. D. Daniels; K. N. Kudin; M. C. Strain; O. Farkas; J. Tomasi; V. Barone; M. Cossi; R. Cammi; B. Mennucci; C. Pomelli; C. Adamo; S. Clifford; J. Ochterski; G. A. Petersson; P. Y. Ayala; Q. Cui; K. Morokuma; D. K. Malick; A. D. Rabuck; K. Raghavachari; J. B. Foresman; J. Cioslowski; J. V. Ortiz; B. B. Stefanov; G. Liu; A. Liashenko; P. Piskorz; I. Komaromi; R. Gomperts; R. L. Martin; D. J. Fox; T. Keith; M. A. Al-Laham; C. Y. Peng; A. Nanayakkara; C. Gonzalez; M. Challacombe; P. M. W. Gill; B. G. Johnson; W. Chen; M. W. Wong; J. L. Andres; M. Head-Gordon; E. S. Replogle; J. A. Pople, *Gaussian 98*, revision A.9; Gaussian, Inc.: Pittsburgh, PA, 1998 (http://www.gaussian.com).

22 T. Helgaker; H. J. Aa. Jensen; P. Jorgensen; J. Olsen; K. Ruud; H. Ågren; A. A. Auer; K. L. Bak; V. Bakken; O. Christiansen; S. Coriani; P. Dahle; E. K. Dalskov; T. Enevoldsen; B. Fernandez; C. Haettig; K. Hald; A. Halkier; H. Heiberg; H. Hettema; D. Jonsson; S. Kirpekar; W. Klopper; R. Kobayashi; H. Koch; K. V. Mikkelsen; P. Norman; T. M. Pedersen; M. J. Packer; Z. Rinkevicius; E. Rudberg; T. A. Ruden; P. Salek; A. Sanchez; T. Saue; S. P. A. Sauer; B. Schimmelpfennig; K. O. Sylvester-Hvid; P. R. Taylor; O. Vahtras. *DALTON, a molecular electronic structure program*, release 2.0; 2005 (http://www.kjemi.uio.no/software/dalton/dalton.html).

